Biophysical Journal
Article

Biophysical Society

Robustness in phenotypic plasticity and heterogeneity patterns enabled by EMT networks

Anish Hebbar,[1] Ankush Moger,[1] Kishore Hari,[2] and Mohit Kumar Jolly[2,*]
[1]Undergraduate Programme, Indian Institute of Science, Bengaluru, India and [2]Center for BioSystems Science and Engineering, Indian Institute of Science, Bengaluru, India

ABSTRACT Epithelial-mesenchymal plasticity (EMP) is a key arm of cancer metastasis and is observed across many contexts. Cells undergoing EMP can reversibly switch between three classes of phenotypes: epithelial (E), mesenchymal (M), and hybrid E/M. While a large number of multistable regulatory networks have been identified to be driving EMP in various contexts, the exact mechanisms and design principles that enable robustness in driving EMP across contexts are not yet fully understood. Here, we investigated dynamic and structural robustness in EMP networks with regard to phenotypic heterogeneity and plasticity. We use two different approaches to simulate these networks: a computationally inexpensive, parameter-independent continuous state space Boolean model, and an ODE-based parameter-agnostic framework (RACIPE), both of which yielded similar phenotypic distributions. While the latter approach is useful for measurements of plasticity, the former model enabled us to extensively investigate robustness in phenotypic heterogeneity. Using perturbations to network topology and by varying network parameters, we show that multistable EMP networks are structurally and dynamically more robust compared with their randomized counterparts, thereby highlighting their topological hallmarks. These features of robustness are governed by a balance of positive and negative feedback loops embedded in these networks. Using a combination of the number of negative and positive feedback loops weighted by their lengths, we identified a metric that can explain the structural and dynamical robustness of these networks. This metric enabled us to compare networks across multiple sizes, and the network principles thus obtained can be used to identify fragilities in large networks without simulating their dynamics. Our analysis highlights a network topology-based approach to quantify robustness in the phenotypic heterogeneity and plasticity emergent from EMP networks.

SIGNIFICANCE Epithelial-mesenchymal plasticity (EMP) is a key arm of cancer metastasis. Despite extensive intra- and intertumor heterogeneity, the characteristics of EMP have been observed to be robust across multiple contexts. We hypothesize that topology of EMP regulatory networks contributes toward this robustness. Here, we measure the robustness of EMP in the form of its phenotypic heterogeneity and plasticity and show that EMP networks are more robust to dynamical (change in kinetic parameters) and structural (change in network topology) perturbations compared with their random network counterparts. Furthermore, we propose a network topology-based metric using the length of feedback loops that explains the observed robustness. Our metric hence serves to quantify robustness in multistable EMP networks without simulating their dynamics.

INTRODUCTION

Robustness is an inherent property of many biological systems and a fundamental feature of evolvability (1,2). Robust systems can maintain their functions or traits despite a dynamically changing environment, and thus possess enhanced fitness (3). Trait robustness is pervasive in biology throughout at many organizational levels, including protein folding, gene expression, metabolic flux, physiological homeostasis, development, organism survival, species persistence, and ecological resilience (4–6). At the cellular level, only a limited number of specific internal/environmental changes lead to a change in the otherwise robust cell fate. Waddington (7) postulated that mechanisms have evolved that stabilize a phenotype against both genetic and environmental perturbation. He called this process "canalization" and contrasted it with developmental "flexibility" in which a phenotype changes, adaptively, with a change in environment. Thus,

Submitted March 9, 2022, and accepted for publication July 11, 2022.
*Correspondence: mkjolly@iisc.ac.in
Anish Hebbar and Ankush Moger contributed equally to this work.
Editor: Alex Mogilner.
https://doi.org/10.1016/j.bpj.2022.07.017

understanding the mechanisms underlying robustness is of fundamental importance.

The study of robustness is also an integral part of various engineering and socio-ecological systems (8,9). Designing robust machines involves integrating specific interactions (feedbacks, for example) between the individual components, forming intricate networks. Similarly, biological systems, such as cells or organisms, also have underlying networks, with interactions that have evolved over millions of years that can impart emergent properties, such as robustness to the biological system. Examples of these networks include metabolic networks, protein interaction networks, gene regulatory networks (GRNs), etc. (10–13). The complexity of the interactions in these networks leads to emergent properties, which manifest as traits of the biological system. In such networks, robustness can be studied in two ways, as classified by the nature of perturbations made to the network. Structural robustness is the study of robustness of biological traits to changes in the underlying regulatory network topology, such as edge deletions, caused by strong perturbations, such as genetic mutations (14). Dynamical robustness, on the other hand, is the study of robustness of traits to changes in the parameters governing the dynamics of the components or nodes of the regulatory networks (production and degradation rates, link strengths, etc.) (15).

Depending upon the system of study and the question of interest, the properties for which robustness is studied might differ. Two such properties of interest in multistable cell fate decision-making networks are phenotypic distribution and plasticity. Phenotypic distribution refers to the collection of phenotypes (gene expression patterns for a transcriptional GRN, for example) that the network can exhibit under different conditions or parameters. An understanding of the factors controlling these distributions for a biological system can lead to the power of manipulating the fate of said biological system despite the ever-present heterogeneity in the system. Plasticity, on the other hand, refers to the ability of the network to adapt to a changing environment by modifying its phenotype, a crucial ability in many systems, such as cellular differentiation and cancer metastasis. The concepts of phenotypic plasticity and heterogeneity (distribution) are well represented by Waddington's epigenetic landscape (7) in which valleys denote gene expression patterns (phenotype) that can switch back and forth under the influence of noise or other external perturbations (Fig. 1 *a*).

To understand robustness, a variety of mathematical models have been used. For example, building on the concept of canalization by Waddington, Kauffman introduced a version of this concept to Boolean network modeling of GRNs by studying canalizing functions (16). In the past decade, the mathematical frameworks for characterizing the robustness of networks have been studied in various settings, such as directed networks, embedded networks, and many more (11,17,18). Robustness has been widely investigated in linear control systems (19,20), but it remains very difficult to measure the robustness of complex nonlinear systems (21). More recently, investigations of how some network topological metrics may associate with the robust behavior of biological systems has been carried out (22,23). However, such investigations are limited in number as well as in the scope of their generality. Hence, a comprehensive and scalable understanding of the role of network topology in robustness is required.

Here, we demonstrate the structural and dynamic robustness of the GRNs underlying epithelial-mesenchymal plasticity (EMP) (Fig. 1 *b*). EMP is a fundamental cellular process implicated in development, wound healing, and cancer metastasis (24,25). Its robust and tightly controlled dynamics have been recently investigated using quantitative experimental data and associated mathematical models (26–28). Particularly, cells exhibiting EMP can both display a wide spectrum of phenotypes as well as plasticity (switching) among them spontaneously (29,30). What remains unclear though is what factors contribute to robustness in phenotypic plasticity and heterogeneity dynamics. We hypothesize that this robustness is an emergent property of underlying regulatory networks. To test this hypothesis, we used a parameter agnostic, ODE-based formalism, RACIPE, and a parameter-independent continuous framework. We investigated the characteristics of robustness in phenotypic heterogeneity and plasticity and identify underlying unifying trends. Particularly, we find that the number of positive and negative feedback loops (NFLs) in the system govern the extent of robustness in phenotypic distribution and plasticity. We also use this framework to predict which links in a network can be targeted and modified to inhibit plasticity—which may provide therapeutic insight in the clinic for targeting EMP. Our results thus provide an integrated understanding of the design principles that enable robustness in multistable EMP networks.

RESULTS

Measuring the robustness of EMP networks

To investigate robustness in EMP, we considered various GRNs underlying EMP (Figs. 1 *b* and S1a) (26). Each network has a set of activating (pointed arrows) and inhibiting (hammer-head arrows) edges/links connecting the nodes of the network. These activating and inhibiting interactions are modeled using ODE formalism, where varying strength of these interactions alter the production rates of corresponding target nodes. We focus on two emergent dynamical outputs of a given GRN: phenotypic heterogeneity (frequency distribution of different discretized steady states/phenotypes) and plasticity (fraction of randomly chosen parameter sets in ODE simulations that can give rise to multiple steady states). We then make different types of perturbations to these

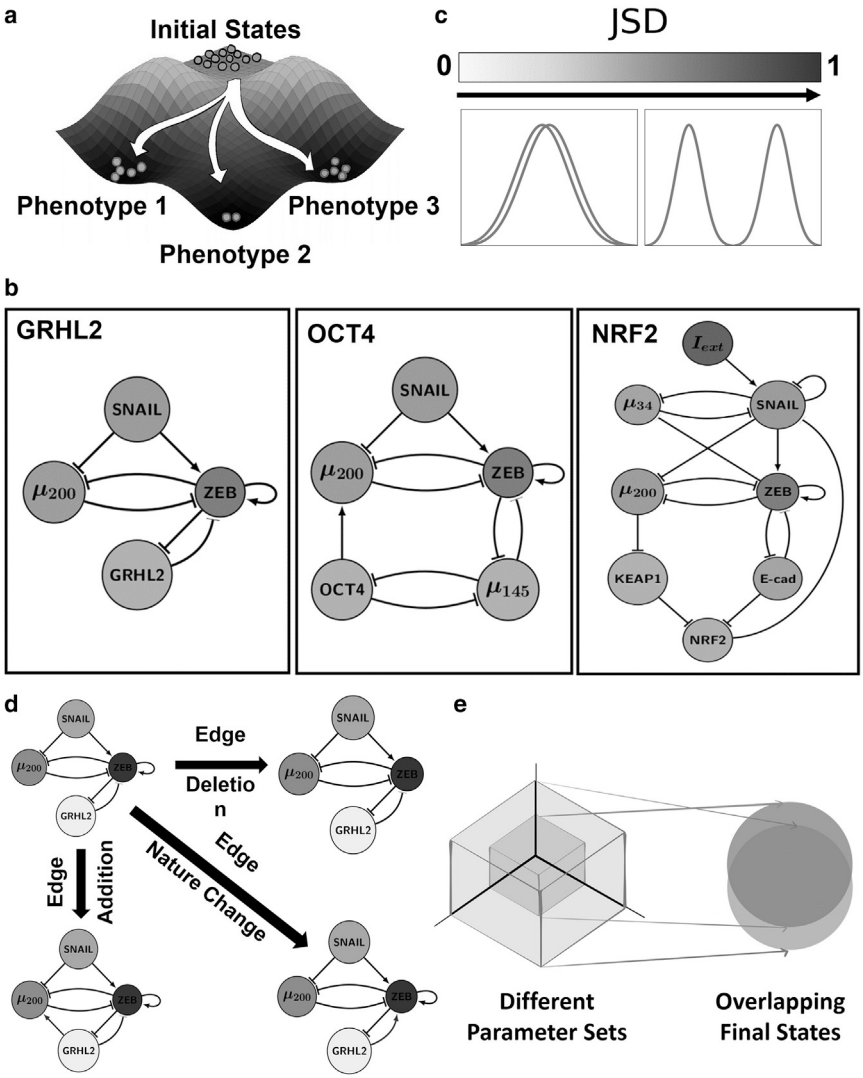

FIGURE 1 Measurement of robustness in multistable biological networks. (*a*) Depiction of plasticity as the ability of a system (defined by a set of parameters) to achieve multiple phenotypes depending on the initial state. (*b*) EMP networks analyzed, namely GRHL2 (4 nodes, 7 edges), OCT4 (5 nodes, 10 edges), and NRF2 (8 nodes, 16 edges). (*c*) Demonstration of how JSD between two frequency distributions varies; JSD ranges from 0 to 1. (*d*) Different ways to perturb the topology/structure of a network: deletion of an edge, addition of an edge, edge nature change from activation to inhibition and vice versa. (*e*) Depiction of dynamic robustness where different parameter spaces converge to largely overlapping solution space.

networks and measure the changes in these outputs, such that smaller changes indicate robustness of the network. Specifically, the change in phenotypic distribution upon perturbations is measured via an entropy-based information theoretical metric called Jensen-Shannon divergence (JSD) (31) (see Methods and Fig. 1 *c*). JSD varies between 0 and 1, where 0 indicates identical distributions, whereas 1 indicates nonoverlapping distributions. The change is plasticity is measured using a modified fold-change formula (for two networks 1 and 2, the fold change is $min(p1/p2, p2/p1)$, where *p1* and *p2* are plasticity measures of both networks). This fold change varies between 0 and 1, and the closer it gets to 1 the more robust the network. Notice that both JSD and fold change only describe the quantity of the change and not the direction of it. The direction of the change in plasticity (is $p_1/p_2 > 1$ or < 1?) and phenotypic distribution (which states see an increased/decreased frequency?) are not explicitly investigated here.

We measured robustness of EMP networks to two kinds of perturbations: structural and dynamical. Structural perturbations are changes to the network topology carried out one edge at a time. This can be edge deletion, addition or nature change (activation to inhibition and vice versa) (Fig. 1 *d*). Dynamical perturbations are changes carried out to the parameter space in which the network is simulated (Fig. 1 *e*), such as modification of the parameter space by changing the range of the parameters considered in ODE simulations, or completely eliminating parameters while simulating network dynamics (Boolean simulations). Correspondingly, structural or dynamical robustness of a network is defined as the average change in an output (JSD or fold-change in plasticity) obtained upon making structural or dynamical perturbations to the network. A small value of average change in the output will be considered as the network being structurally or dynamically robust with respect to that output (Fig. 1 *e*).

EMP networks are dynamically robust

We simulate each network using an ODE-based framework called RACIPE (32) (see supporting material). For a given GRN, the framework first constructs a set of coupled ordinary differential equations. Then, multiple sets of ODE parameters are generated from predetermined ranges (the parameter space), which are then used to simulate interactions between nodes of the network. These simulations can be used to identify the robust dynamical features of a particular network. Because RACIPE randomly samples parameters for each simulation, it can be thought of as a parameter agnostic framework (32). Using this framework, we can analyze the dynamic robustness of a network by studying the variation in network behavior with changes in RACIPE parameter space (dynamic perturbation). Plasticity score of the network is then defined as the fraction of such random parameter sets that can give rise to multiple stable states (26). The phenotypic distribution is calculated by discretizing the steady states obtained for each parameter set (see supporting material for discretization procedure) in RACIPE simulations and calculating the frequency of these states over the parameter space.

Because the network behavior in RACIPE is regulated by both network topology and various kinetic parameters, plasticity and phenotypic distribution can vary across distinct parameter ensembles. Therefore, to measure the dynamic robustness of these networks, we first simulated these EMP networks using RACIPE by varying the maximum ranges for different network parameters via multiplying them by a factor ranging from $1/3$ to 3, thereby varying the parameter space. While multiplication factor > 1 leads to the expansion of the parameter space, multiplication factor < 1 shrinks the parameter space. We then measured the JSD and fold change in plasticity obtained from dynamically perturbing this system for all EMP networks. The maximum JSD obtained for any EMP network was 0.25 upon such dynamic perturbation (Fig. S2, *a* inset, *c*, and *d*). Furthermore, phenotypic distribution seems more sensitive to shrinking the parameter space than to expansion of parameter space. Similarly, plasticity also was seen to be sensitive to shrinking the parameter space than to expanding it, and particularly to changes in Hill coefficient (Fig. S2, *b*, *e*, and *f*).

Given our hypothesis that the network topology can lead to robustness in EMP, if we generate random network topologies of similar sizes as that of the EMP networks and subject them to dynamical perturbations, the average change in outputs obtained should be more than that of the EMP networks. Hence, we generated three sets of 100 random (hypothetical) networks each for the sizes of 4 nodes, 5 nodes, and 8 nodes, respectively (Methods). In this context, we refer to the EMP networks as wild-type (WT) networks. We then perturbed these networks dynamically in the same manner as described in the previous paragraph, and calculated the average JSD and average fold-change in plasticity calculated across all multiplication factors of the RACIPE parameter space. The distribution of these values, when plotted, revealed that WT networks had much lower JSD, and an average fold change in plasticity much closer to 1 than most of the random networks (Fig. 2, *a–f*). Moreover, the percentiles of the WT networks in the histograms were consistent across all three runs (reported in the plots as mean $\pm$ SD in Fig. 2), further reinforcing that the EMP networks are more dynamically robust than their random counterparts.

Another way to understand the variation due to kinetic parameters is to compare the network behavior in RACIPE simulations with that of a parameter-independent framework, such as Boolean (logical) formalism (33). The dynamics of Boolean models are governed purely by the topology of the network. The gene activities are discrete (either ON or OFF), which gives us a more qualitative understanding of how the nodes in the network influence each other to give rise to varying network dynamics. Therefore, Boolean formalism can serve as a nonparametric counterpart to RACIPE formalism. Note that, with Boolean formalism, we cannot define plasticity in the way we define it for RACIPE; therefore, only robustness in phenotypic distribution can be studied.

We applied a threshold-based Boolean formalism (33) to simulate these networks (see supporting material). While the top states obtained from both formalisms are the same for WT EMP networks, dissimilarity between the steady-state distributions obtained in both frameworks is relatively large ($JSD \sim 0.5$, Fig. S3, *a–d*). While this range of JSD values could indicate lack of dynamic robustness in EMP networks, we asked if the high dissimilarity between RACIPE and Boolean might be confounded by the differences between the methods, other than the lack of parameter sets in the latter. Hence, we sought to eliminate these confounding variables by modifying the Boolean formalism.

The existing Boolean formalism differs from RACIPE in two aspects: the lack of kinetic parameters compared with RACIPE and it operates in a discrete state space instead of a continuous one. Thus we decided to modify Boolean formalism by making its state space continuous (Fig. 3 *a*). The details of the implementation of this formalism, termed continuous state space Boolean (CSB) formalism, are given in the Methods section. This formalism provides a better measure of the dynamic robustness of the networks, because the essential difference between the CSB formalism and RACIPE is the lack of kinetic parameters in the former, so any differences that arise must be from these kinetic parameters. While this formalism is parameter independent, the steady-state phenotypic distributions obtained in this model are much closer to that obtained via RACIPE (lower JSD), relative to the earlier Boolean model, for all EMP networks (Figs. 3 *a* and S4, *a*, and *b*). Most random (hypothetical) networks showed this increased similarity as well (Fig. 3 *c*), suggesting that this framework can be applied to a larger

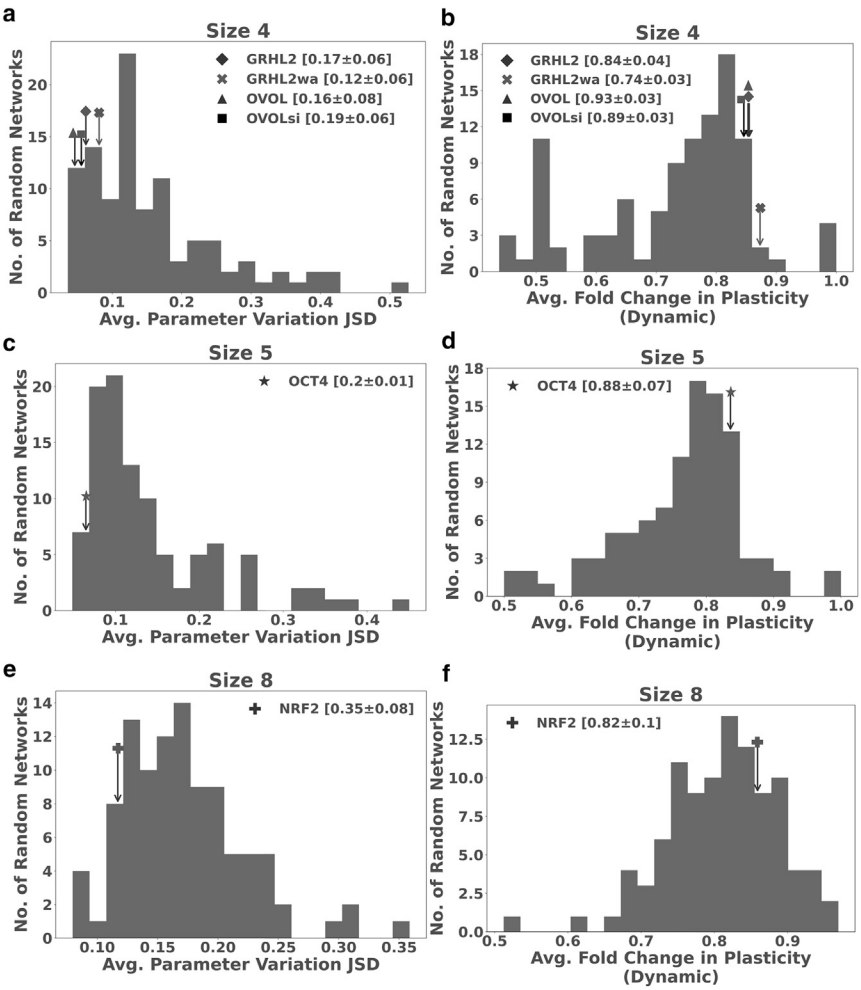

FIGURE 2 High dynamical robustness of EMP networks. (*a*) Histogram of average JSD for random networks of size 4, with corresponding EMP networks marked with arrows with different shapes at their tail. Percentiles for WT networks reported as mean ± standard deviation. (*b*) Similar to (*a*), but for average fold change in plasticity. (*c* and *d*) Similar to (*a*) and (*b*) but for random networks of size 5, with corresponding EMP network marked with an arrow. (*e* and *f*) Similar to (*a*) and (*b*), but for random networks of size 8, with corresponding EMP network marked with an arrow.

set of networks. Moreover, this model is computationally inexpensive compared with RACIPE as measured for simulations across varying network sizes (Fig. S4 *c*). We also saw that the results obtained in the CSB are more consistent for the same number of simulations when compared with RACIPE, further highlighting its benefits as an alternative to ODE-based methods (Fig. S4 *d*).

Using the CSB formalism, we then simulated the WT as well as the random networks and obtained the JSD between the phenotypic distributions of RACIPE and CSB for each network. Similar to the previous case of perturbation of parameter space, WT EMP networks show a lower JSD than most of their random network counterparts, reinforcing that EMP networks are dynamically robust (Fig. 3, *d–f*).

Structural robustness of multistable EMP networks

We then tried to understand if EMP networks are structurally robust. We perturbed the WT as well as the random networks one edge at a time, exhaustively, in the manner depicted in Fig. 1 *d*. We then proceeded to simulate each network (WT and random) and its perturbed counterparts using RACIPE and CSB, with the aim of deriving measures of robustness. However, RACIPE simulations for networks of size greater than 8 proved computationally quite expensive. Given the similarity between the phenotypic distributions of RACIPE and CSB, we wanted to ask if the similarity holds for the perturbed counterparts as well. For WT EMP networks, we find a very strong correlation between the perturbation JSD (pJSD between the phenotypic distributions of unperturbed and perturbed networks) obtained from RACIPE and that obtained from CSB (Figs. 4, *a*, *b* and S5, *a–g*). Because CSB is computationally cheaper than RACIPE (Fig. S4 *c*) and the pJSD obtained from RACIPE is very close to that of CSB, we chose to use CSB to measure structural robustness of EMP networks in phenotypic distribution.

We simulated the WT and random networks and their perturbations using the CSB formalism, and calculated the pJSD for each perturbed network as described in the previous paragraph. For instance, for the GRHL2 network, we plotted this distribution of pJSD values (Fig. 4 *c* inset).

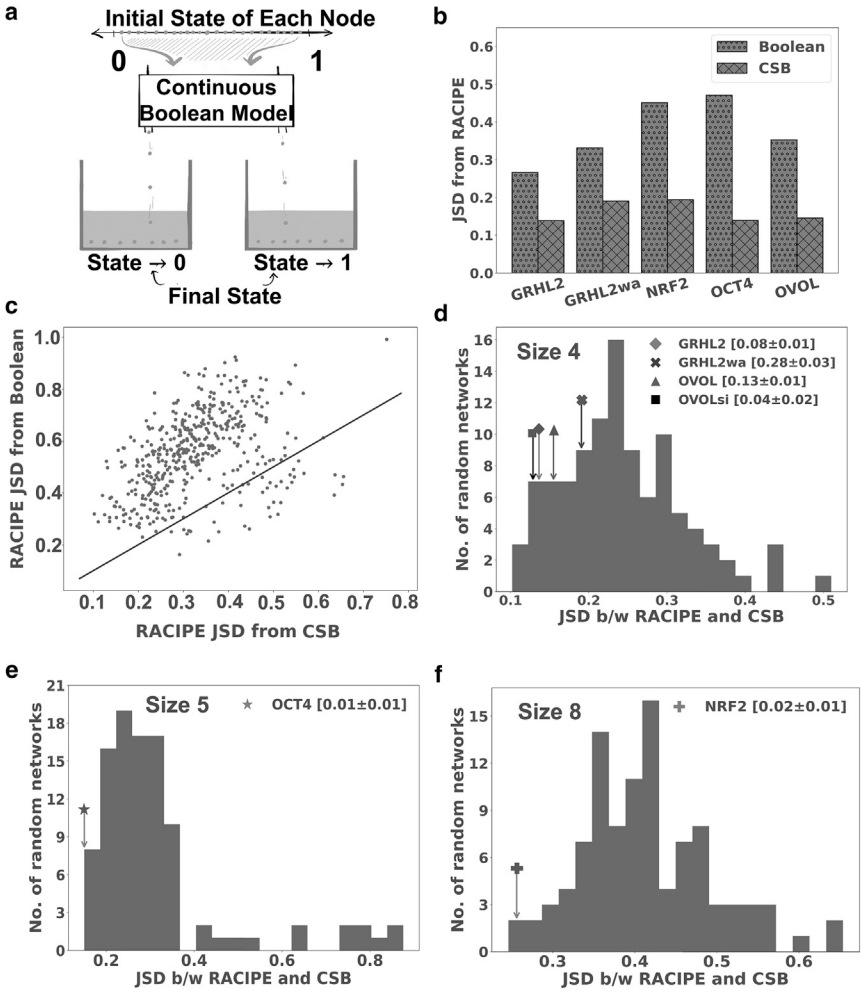

FIGURE 3 Continuous state space Boolean (CSB) formalism captures the dynamic robustness of EMP networks. (*a*) Visualization of the CSB framework. Networks are simulated in a continuous state space and the resultant final states are discretized. (*b*) Comparison of JSD of the phenotypic distributions obtained by RACIPE from the Boolean framework (dotted bars) and CSB framework (cross-patterned bars) for various EMP networks. (*c*) Comparison of JSD of the phenotypic distributions obtained from RACIPE against those obtained from CSB formalism (*x* axis) and Boolean formalism (*y* axis). The line represents $x = y$. (*d*) Histogram of average JSD for random networks of size 4, with corresponding EMP networks marked with arrows. Percentiles for WT networks reported as mean ± standard deviation. (*e*) Same as (*d*), but for networks of size 5. (*f*) Same as (*e*), but for networks of size 8.

We then took an average of these JSD values to represent the structural robustness of a given network. The distribution of the average pJSD values for random networks revealed that the EMP networks have a lower average pJSD and therefore higher structural robustness in phenotypic distribution compared with most random networks when perturbed similarly (Figs. 4, *b*, *c*, and S5h). However, single edge perturbations may not fully capture the robustness landscape, as it is also possible to modify multiple edges at the same time. Consequently we investigated the effect of multiple edge perturbations in the EMP networks (Fig. S6, *b* and *c*). If a network has E number of edges, we performed up to E number of random edge perturbations to see how the average JSD varies with perturbation size. We observed that the average pJSD for a single edge was about half of the average obtained in E perturbations, indicating that analyzing the effects due to a single perturbation is sufficient to understand the robustness in phenotypic distribution of a network to edge modifications.

For the analysis of structural robustness in plasticity, we simulated the WT and random networks and the corresponding perturbations using RACIPE, because plasticity is defined only for RACIPE. Similar to JSD, we calculated the average fold change in plasticity for each random network and obtained a distribution of the same. We found that the average fold change in plasticity, obtained from a distribution of the fold change in plasticity upon all topological perturbations (Fig. 4 *c* inset) of WT networks is closer to 1 than that of most random networks (Fig. 4, *c* and *d*), indicating that the EMP networks are structurally more robust than their random network counterparts.

Feedback loops underlie the robustness in EMP networks

After characterizing dynamical and structural robustness in the EMP networks, we attempted to explore the network topological characteristics that lead to robustness in EMP. Positive feedback loops (PFLs) have been reported to play a major role in the stability of biological networks. PFLs reinforce the network such that the nodes involved in the loops are inclined to display similar expression levels

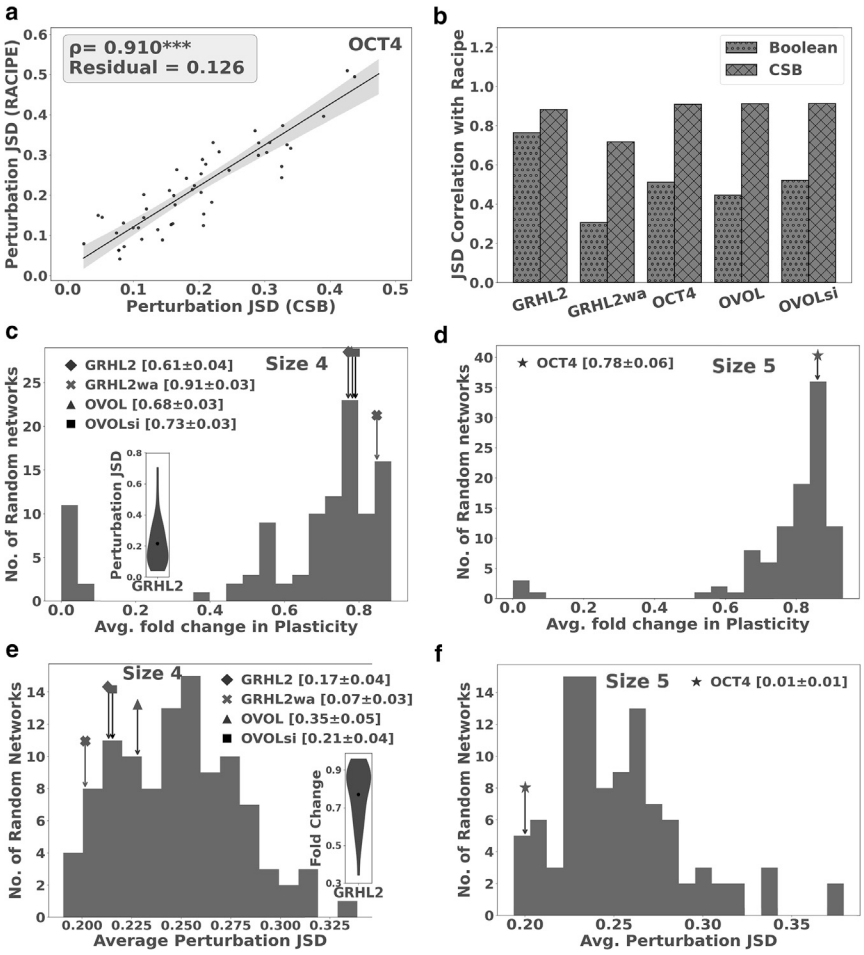

FIGURE 4 Structural robustness and feedback loops. (*a*) Comparison of perturbation JSD obtained via RACIPE (*y* axis) and CSB (*x* axis) for OCT4 network. Each dot represents one perturbed network. The correlation coefficient and the residual for linear fit has been reported, with the p value for correlation to be interpreted as: ***p < 0.001. (*b*) Correlation coefficient between perturbation JSD from RACIPE and perturbation JSD from Boolean (dotted bar) and perturbation JSD from CSB (criss-cross patterned bar). (*c*) Histogram of average perturbation JSD for networks of size 4, with corresponding EMP networks marked with arrows. Percentiles for WT networks reported as mean ± standard deviation. Inset shows the distribution of perturbation JSD for GRHL2 network. (*d*) Same as (*c*), but for random networks of size 5. (*e*) Same as (*c*), but for average fold change in plasticity. (*f*) Same as (*e*), but for networks of size 5.

(34–36). The reinforcement provided by PFLs can lead to convergence to approximately similar steady states across a wide range of parameters in RACIPE. Moreover, PFLs have been shown to play a crucial role in governing the plasticity of the networks as well (26). Similarly, NFLs can contribute to oscillations (34–36). Therefore, we hypothesized that PFLs and NFLs can govern the robustness of these GRNs.

To understand if the PFLs and NFLs play a role in imparting structural and dynamical robustness to networks, we used the ensemble of random networks created. First, we divided the distributions of average pJSD (Fig. 4 *c*) and average fold change in plasticity (Fig. 4 *d*) about their respective medians, and asked if there was a significant difference in the distribution of feedback loops for the networks with high robustness versus those with low robustness. The networks with the lower average pJSD had a significantly higher number of PFLs and a lower number of NFLs, as quantified by the difference in the means of the distributions (Fig. 5 *a*). Interestingly, the shift in the distribution of NFLs is more distinct when compared with that of PFLs. Similarly, the networks with a higher average fold change in plasticity have a smaller number of NFLs and a larger number of PFLs (Fig. 5 *b*). Unlike with JSD, the two groups of networks in case of plasticity are better differentiated by PFLs than with NFLs. These results suggest that PFLs and NFLs might have varying degree of importance in governing different kinds of robustness. A common feature for robustness in both plasticity and heterogeneity (as measured by JSD) seems to be, however, that the networks with higher robustness have a larger number of PFLs and a smaller number of NFLs.

We then asked how well the PFLs and NFLs can explain robustness of any network. To answer this question, we calculated the correlation of the measures of robustness with PFLs and NFLs, across EMP and random networks of all sizes. Structural robustness in plasticity is strongly correlated with the number of PFLs in a network (Fig. 5 *c*). However, correlation with the number of NFLs is very weak and not statistically significant. While NFLs show a better correlation with dynamical robustness in plasticity (obtained by varying the parameter space), the strength is still weaker than PFLs (Fig. S6, *a* and *b*), suggesting that PFLs can explain robustness in plasticity better than

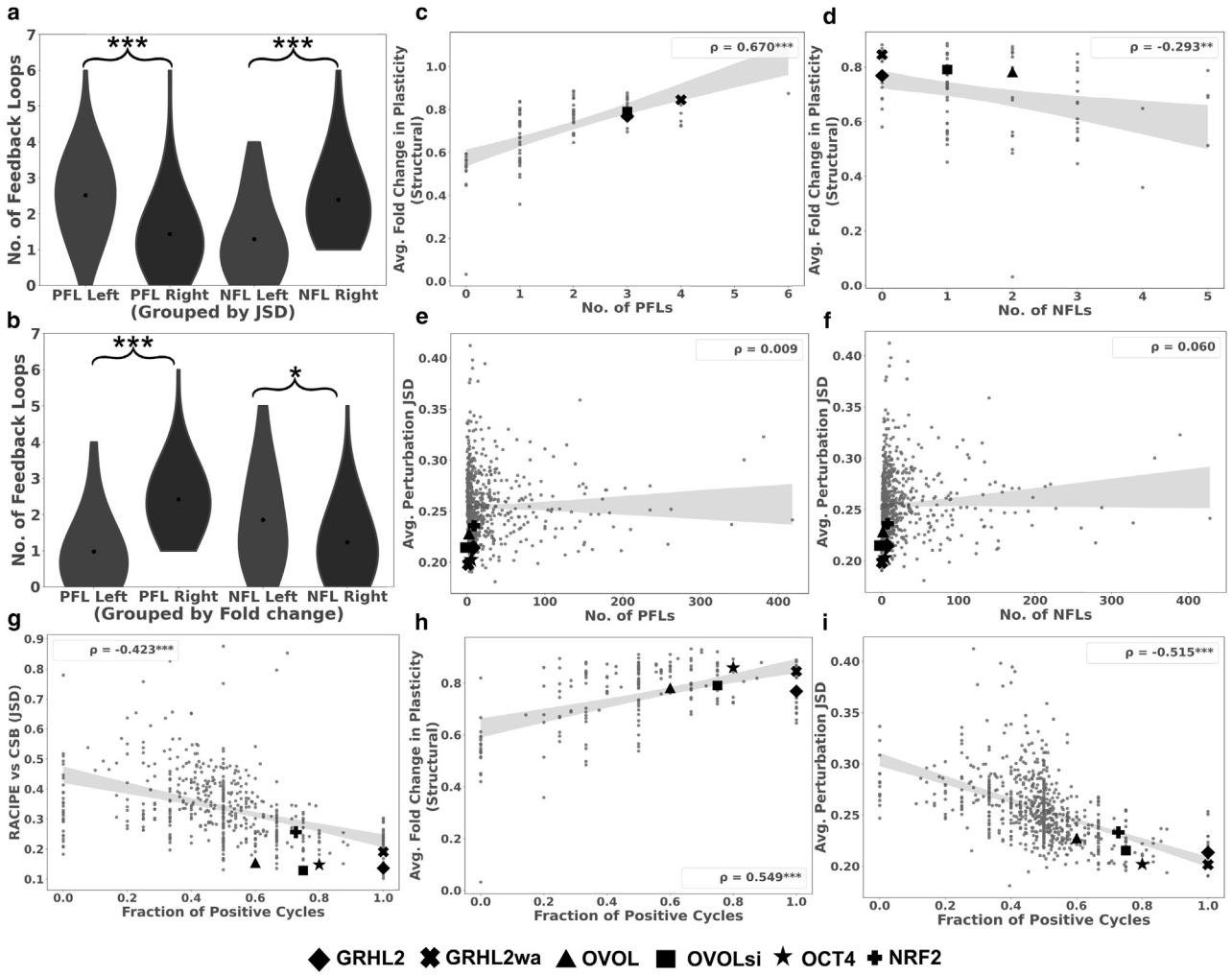

FIGURE 5 Feedback loops can explain the robustness of EMP networks. (*a* and *b*) Violin plots depicting the distribution of negative feedback loops (NFLs) and positive feedback loops (PFLs) on either side of the median of the histograms in Fig. 4, *c* and *e*, respectively. Unpaired t test comparing the distribution of feedback loops on either side of the median was performed, with significance depicted on top of the plots. (*c* and *d*) Scatterplot of the average fold change in plasticity upon structural perturbation (structural robustness in plasticity) (*y* axis) and number of PFLs (*c*) and the number of NFLs (*d*). Each dot represents a random network. The WT EMP networks are highlighted using points of different shapes. Spearman correlation coefficient is reported in the legend of both panels, with the p value to be interpreted as: ***p $<$ 0.001. (*e* and *f*) Same as (*c*) and (*d*), but for average perturbation JSD (structural robustness in distribution). (*g*–*i*) Scatterplot between fraction of positive cycles (FPCs, *x* axis) against the robustness measures: (*g*) JSD between the phenotypic distributions obtained from RACIPE and CSB formalisms (dynamical robustness in distribution), (*h*) average fold change in plasticity upon structural perturbations, and (*i*) average perturbation JSD. The WT EMP networks are highlighted using points of different shapes. Spearman correlation coefficient is reported in the legend of each panel. p Values in the figure to be interpreted as: * p $<$ 0.05, ** p $<$ 0.01, ***p $<$ 0.001.

NFLs. On the contrary, dynamical robustness in distribution, measured as the JSD between phenotypic distributions obtained from RACIPE and CSB formalisms, showed a stronger correlation with NFLs than with PFLs (Fig. S6, *c* and *d*, $\rho = 0.417$ vs. $\rho = 0.213$). However, structural robustness in distribution (average pJSD) did not show significant correlations with either PFLs or NFLs.

Clearly, neither PFLs nor NFLs alone can explain all four kinds of robustness observed in EMP networks. Hence, we asked if a combination of PFLs and NFLs can explain robustness better. To that end, we chose the fraction of positive cycles $\left(FPC = \frac{PFLs}{PFLs+NFLs}\right)$ as the metric. In addition to including the effects of both PFLs and NFLs, the fraction of positive cycles (FPC) is also limited between 0 and 1, making it a metric comparable across the networks of various sizes. The FPC loops correlated positively with dynamical robustness in phenotypic distribution (Fig. 5 *g*, negative correlation with JSD), with the strength of the correlation being comparable with that of the number of NFLs ($\rho = 0.423$ vs. $\rho = 0.417$). Similarly, dynamical robustness in plasticity also correlated positively with FPC (Fig. S6 *e*). Structural robustness in plasticity again showed a positive correlation with FPC, with the strength being slightly lesser than that for the number of PFLs (Fig. 5 *h*, $\rho = 0.549$ vs. $\rho = 0.626$). However, structural robustness in distribution, which did not correlate with either of the individual loop

metrics before, correlates very well with the FPC, adding to its utility over individual loop metrics. Furthermore, robustness in all dimensions measured here increases (JSD decreases and fold change in plasticity gets closer to 1) as the FPC increase. Further support to this argument is provided by the fact that the WT EMP networks have a higher FPC than most of the random networks, thereby leading to the higher robustness in these networks (stars in Figs. 5, *g–i* and S6 *e*).

Length-weighted loops serve as a better metric to explain robustness

Previous literature also suggests that not all PFLs play the same role in regulating the plasticity of the network (37,38). Consequently, we decided to adopt another independent weighting strategy: penalize each PFL using its length, i.e., giving a higher importance to smaller feedback loops (see Methods), with the hypothesis that breaking a longer feedback loop would have a lesser effect on the system's output than breaking a shorter feedback loop. We then took a sum over these penalized PFLs, creating a new metric, weighted PFL (WPFL), defined as follows:

$$\mathrm{WPFL} = \sum_i \frac{1}{\mathrm{length}\ (i)}.$$

WPFL showed a better correlation with network plasticity compared with PFLs, supporting WPFL as a better metric (Fig. 6 *a*). The correlation using WPFLs is an improvement on PFLs (most dots are above the $x = y$ line), indicating that it is important to consider the length of the feedback loops as a factor influencing their impact.

Weighing feedback loops by length is an intuitive way of refining the feedback loop metric. We asked if there can be other, nonintuitive ways in which to weight feedback loops. To answer this question, we chose to take a regression-based approach to identify weights to be added to WPFLs that would increase the correlation between the fraction of WPFLs and robustness measures. We first estimated the optimal weights for each network size-robustness measure combination to be assigned to the WPFLs (see supporting material), such that the fraction of WPFLs can be redefined as:

$$FWPC = \frac{w * WPFL}{w * WPFL + WNFL},$$

where w is the optimal weight estimated and WNFL is the length-weighted NFLs. We find that the optimal weights were different for each robustness measure-network size combination (Table 1). We then wanted to see how the strength of correlation (absolute value of the correlation coefficient) changes with different weights given to WPLFs. A visual inspection of the plot of absolute correlations against the weights (Figs. 6 *b* and S7, *a–d*) revealed that, while the optimal weights are different for each robustness metric-network size combination, weights less than 1 generally resulted in poor correlation, whereas any weight greater than 1 showed similar absolute correlation to that of weight = 1. This observation suggests that while the optimal weights might be different, $w = 1$ provides a good correlation

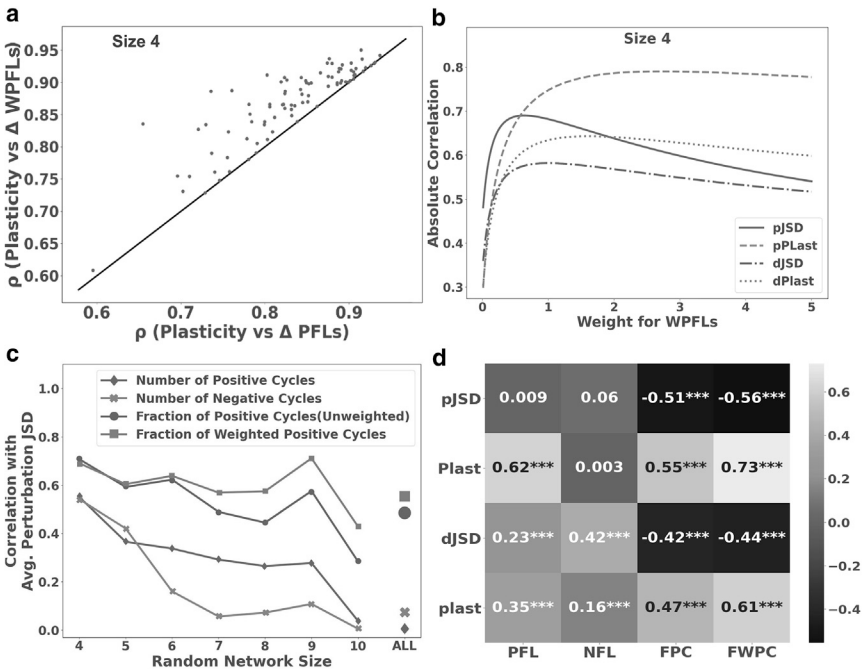

FIGURE 6 Fraction of weighted positive cycles as a measure of robustness. (*a*) Scatterplot of the correlation of plasticity with PFLs and weighted PFLs, along with the $x = y$ line. (*b*) Absolute value of the Spearman correlation b/w average perturbation JSD and PFLs, NFLs, fraction of positive cycles (FPC), and FWPC for networks of different sizes. Absolute values have been used for ease of comparison across robustness measures. (*c*) Change in the strength of correlation between the robustness measures—structural robustness in JSD (pJSD), plasticity (pPlast), dynamic robustness in JSD (dJSD), and plasticity (dPlast)—and FWPC, with change in the weight of WPFL in FWPC, for networks of size 4. (*d*) Heatmap of the correlation coefficients of robustness measures—pJSD, pPlast, dJSD, and dPlast —with PFLs, NFLs, FPC, and FWPC. Statistical significance of correlation is reported as follows: ***p < 0.001.

TABLE 1 Coefficients for WPFL estimated for the calculation of FWPC for various robustness metrics (columns 2–5)

Network size	dJSD	dPlast	pJSD	pPLast
4	0.998	1.598	0.634	2.728
5	0.865	1.38	1.538	5.573
6	1.827	1.814	1.787	
7	1.149	4.125	1.403	
8	2.853	5.957	1.382	
9			1.748	
10			0.064	
All	0.427	2.379	0.933	4.486

strength, which is closer to the maximum possible correlation that can be obtained. In other words, while there may be other ways to weight the feedback loops, length-based weighing captures most of the effect of feedback loops on robustness. Hence, we could redefine the fraction of weighted positive cycles (FWPC) metric as:

$$FWPC = \frac{WPFL}{WPFL + WNFL}.$$

The FWPC metric showed stronger correlations than PFL, NFL, and FPC metrics, across network sizes. We show a representative case for the same in Fig. 6 *c* for structural robustness in JSD, as the correlation of average pJSD with PFLs and NFLs was very low (Fig. 5, *e* and *f*). We then compared the correlation strengths of all four measures of robustness against the four topological metrics across networks of all sizes, and found the FWPC outperforming PFLs, NFLs, and FPCs (Figs. 6 *d* and S7,*e* and *f*).

FWPC can identify fragilities in large networks

To test the scalability of our results, we analyzed 2 large EMP networks: EMT RACIPE (22 nodes, 82 edges) (39) and EMT RACIPE2 (26 node, 100 edges) (40) (Fig. 7, *a* and *b*). We first found the phenotypic distributions of these networks in all three models, RACIPE, Boolean, and CSB (Fig. S8, *a–d*). As it was with the small networks, the CSB showed a better agreement with RACIPE than Boolean. We also found the distribution of multistability (parameter sets giving rise to n steady states, $n = 1,2,3 \ldots$) in RACIPE for these networks (Fig. 6, *c* and *d*) via 100,000 simulations in triplicates. We observed that these networks have very high plasticity, with only up to 5% of parameter sets displaying monostability, the rest being multistable. Note that the error bars in these simulations are very small, showing that the number of simulations performed give an accurate depiction of the fraction of multistable states. We then perturbed these networks structurally (single edge deletions/nature changes, 144 and 202 perturbations respectively) to study their robustness in plasticity. Both of these networks have a large number of PFLs (>3000 and >10,000, respectively), and most perturbations only caused minor change in the plasticity score, thereby demonstrating the structural robustness of these networks. We found the plasticity scores for each of the perturbed networks and, as observed in the networks of smaller scale, the correlation between the plasticity of the perturbed network, and the corresponding change in the number of PFLs was positive and significant (Fig. 7, *e* and *f*) (see Methods for details on these metrics).

However, in both networks there were two perturbations (Fig. 7, *e* and *f*; marked with arrows) that reduced the number of PFLs equally drastically, yet showed different fold change in plasticity. We then plotted the fold change in plasticity against the change in FWPC, and found that the metric showed stronger correlation with plasticity in comparison with the number of PFLs and was able to clearly identify the fragility in the networks that can cause maximum perturbation in plasticity (Fig. 7 *g* and *h*, marked with arrows). These results hence suggest that the FWPC can be used to understand the robustness (and fragility) of larger networks as well.

To establish a causal connection between FWPCs and structural robustness of networks, we perturbed the NRF2 network and a few random networks of same size as that of NRF2 (but with altered topology as a control case). For each network, we identified the edge perturbations that led to the maximum increase or decrease in FWPC for these networks. We then continued to make iterative perturbations that lead to further increase in FWPC value until it reached 1 (or decrease in it until it reached 0) (Fig. 8, *a* and *b*). Our results suggest that reduction in FWPC associates with lower network robustness and vice versa. We measured the structural robustness by calculating the JSD (using the CSB model) for each of these perturbations in both NRF2 and multiple random networks. We found a monotonous decrease in pJSD with an increase in FWPC (Fig. 8, *c* and *d*) both for NRF2 and for a representative random network. Similar monotonic trends between structural robustness and FWPC were observed for other random networks of eight nodes as well (Fig. 8, *e* and *f*). These results strengthen our previously shown correlation-based associations that perturbations made to increase the FWPC metric make the network more robust.

DISCUSSION

Robustness is a fundamental, ubiquitous feature of biological systems, which enables them to maintain their function in fluctuating environments against both dynamic and structural perturbations. Decoding what regulatory network motifs can protect network dynamics against such perturbations is key to understanding robustness. Our results provide a theoretical toolset to identify robustness in both phenotypic distribution and plasticity in multistable EMP networks using a network topology-based approach. We have simulated multiple EMP networks along with an ensemble of their random network counterparts to identify the design

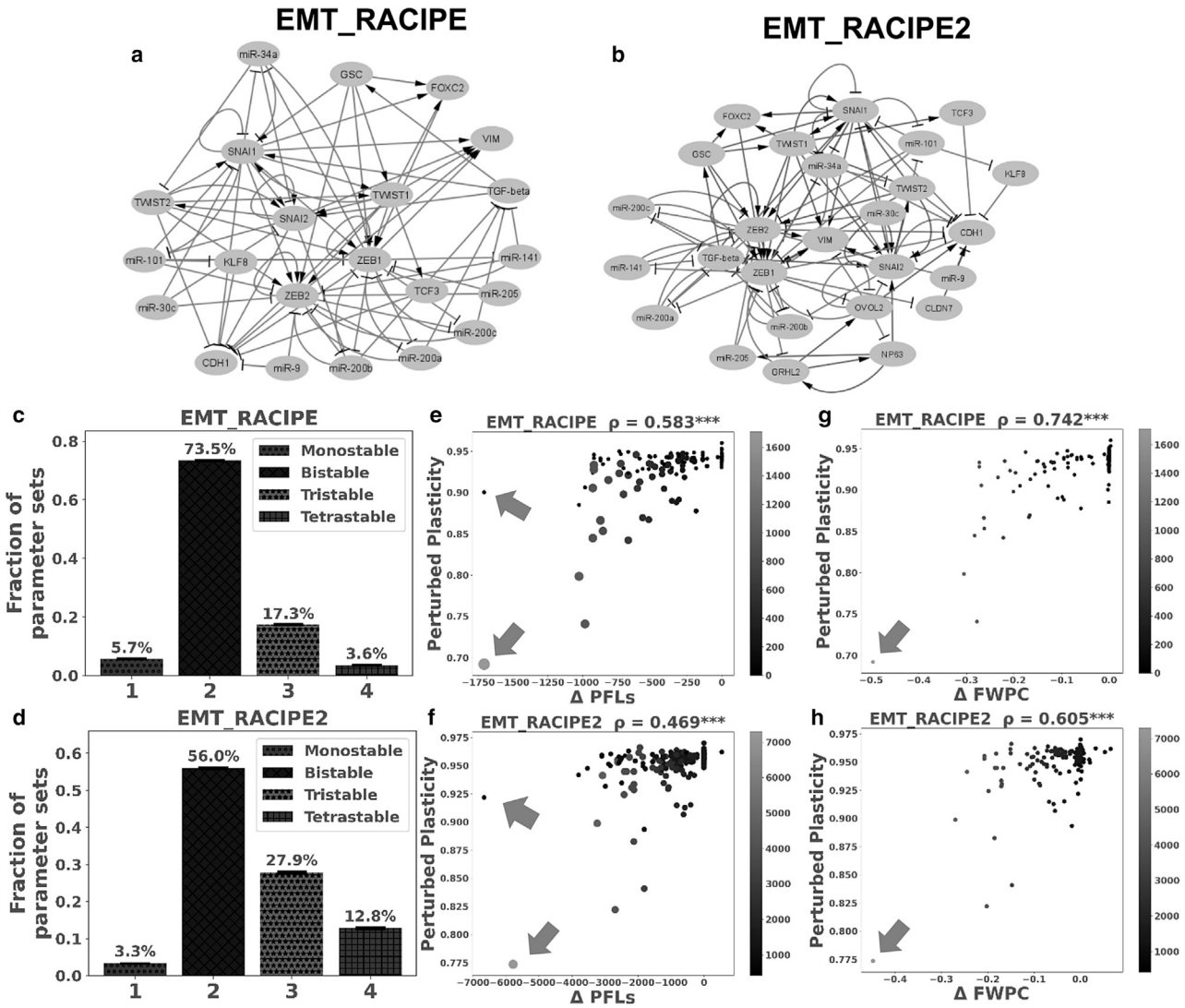

FIGURE 7 Feedback loop-based metric explains robustness in large-scale networks. (*a* and *b*) The 22 node EMP network (EMT_RACIPE) and 26 node EMP network (EMT_RACIPE2). (*c* and *d*) Barplot of the fraction of multistable parameters in RACIPE for EMT_RACIPE, EMT_RACIPE2. Error bars represent the standard deviation of the fraction obtained over 3 replicates. (*e* and *f*) Plasticity of the perturbed network versus change in PFLs for each perturbed network (EMT_RACIPE, EMT_RACIPE2) was plotted. The size of each point represents the number of negative feedback loops. (*g* and *h*) Same as (*e*) and (*f*), but for change in FWPC. Color bar denotes number of negative feedback loops in a given perturbed network topology. Significance of correlation is reported: ***$p < 0.001$.

principles that enable these networks to display robustness when subjected to dynamic or structural perturbation. By understanding design principles of robustness, we also pave way to unearthing the fragilities of the network that can be targeted to significantly perturb phenotypic distribution and plasticity emergent from a given network. We were able to identify the topology-based robustness metric, a weighted fraction of PFLs and NFLs, and showed that when perturbations reduce this metric both the structural and dynamical robustness of the network decreases.

EMP dynamics have been extensively investigated using mathematical models. While smaller regulatory networks are modeled using continuous ODE-based frameworks (27,41), larger networks are modeled using discrete/logical approaches due to lack of scalability of ODE approaches in scenarios where network parameters may not be easily obtained (33). While either formalism may reveal at least the most frequent steady state, a comparative analysis for larger networks becomes computationally quite expensive. Hence, we offer an alternative modeling framework, which is continuous in nature yet parameter independent. This framework is computationally more efficient, offers more detailed analysis compared with the Boolean formalism and can reveal the underlying design principles of a network topology even for larger networks.

In our previous work (26), we observed that the more PFLs in an EMP network, the higher its plasticity. Interestingly, our current study shows that, besides increasing plasticity,

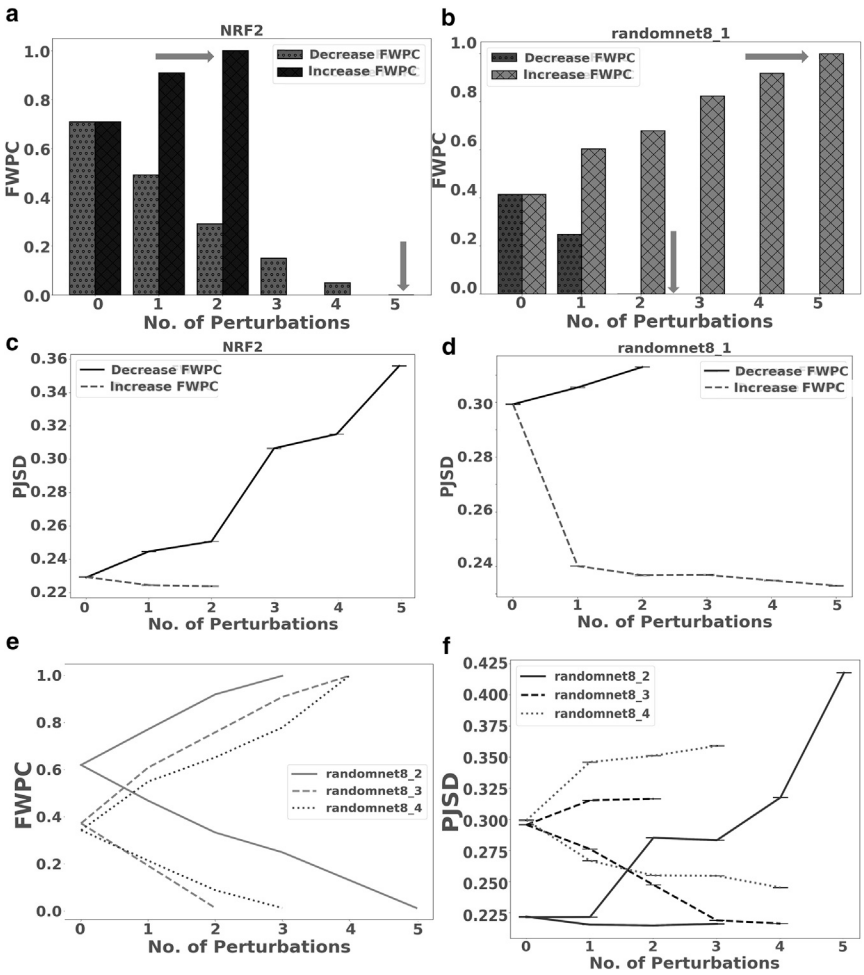

FIGURE 8 Perturbations reducing FWPC reduce network robustness and vice versa. (*a* and *b*) Representative barplot showing the edge perturbations that increase or decrease FWPC maximally iteratively. The arrows show the point at which perturbations were stopped, when either the maximum (1) or minimum (0) FWPC were reached. (*c* and *d*) Change in perturbation JSD for NRF2 and a representative random network of size 8 with each perturbation described in (*a*) and (*b*). (*e*) Change in the FWPC metric with network perturbation for three additional random networks. (*f*) Change in structural robustness (perturbation JSD) with network perturbation for three additional random networks. In (*c*), (*d*), and (*f*); mean ± standard deviation across three replicates are reported.

a higher number of PFLs can also enhance the structural and dynamical robustness of plasticity to various perturbations in network parameters/topology. This has important implications in PFLs as a target for metastasis, as this suggests that an increase in PFLs can maintain the heterogeneity in network dynamics despite fluctuations in the environments. For instance, breaking the positive (mutually inhibitory) feedback loop between miR-200 and ZEB using CRISPR/Cas9 led to reduced metastasis in vivo (42). A finer analysis in this direction would, however, require considering the actual fold change in plasticity which would indicate a decrease or increase in plasticity upon perturbations, thereby telling us if the plasticity increases upon perturbation for networks with lower number of PFLs. Another useful addition would be to characterize plasticity by identifying the specific phenotypes each parameter set is capable of accessing, thereby answering the question of how changes in plasticity change the frequency of hybrid phenotypes, which are crucial to metastasis. Preliminary analysis shows, for WT EMP networks, an increase in hybrid phenotypes as plasticity decreases (43).

We observed that EMP networks were relatively more dynamically robust compared with the random networks of the same size that we had generated. These results reinforce previous observations seen in regulatory networks of other biological contexts. The biochemical network involved in the establishment of segment polarity in *Drosophila melanogaster* has been shown to be robust against changes in initial values and rate constants of molecular interactions, enabling stable pattern formation (44,45). Similarly, in a rewiring experiment for GRN of *E. coli*, wherein new regulatory interactions were added to GRNs, (46) 95% of these modified gene interaction networks were tolerated by the bacteria and some conferred selective advantages in particular environments. Our analysis of the structural robustness of EMP networks reveals similar trends, in terms of both plasticity and phenotypic heterogeneity.

On further analysis of the topological properties that lend these networks dynamical and structural robustness, we found that robustness was associated with having a larger number of PFLs and a smaller number of NFLs. Moreover, the relative importance of each feedback loop was found to vary with both length across the different robustness measures. While other ways to define the importance of a feedback loop might exist, we find that length-based weighing is sufficient to explain robustness in EMP networks. Multiple

studies have modeled the evolution of biological networks, selecting for fitness (47), randomly generating GRNs using Markov chain Monte Carlo (48), and using preferential attachment (34), finding that robust networks are rich in PFLs and have relatively lower number of NFLs. Furthermore, the robustness offered due to these motifs can be evolutionarily stable (49) to edge perturbations, thereby possibly explaining the robustness of EMP in multiple biological contexts. Studies have also identified patterns in complexity, such as teams of nodes that impart structural and dynamical robustness in EMP networks (50). It is important to identify the connections between the role of PFLs and NFLs in such patterns.

Our methods only investigate robustness on the gene regulatory level; however, it is important to understand how the interactions between genes, proteins, and metabolites contribute to robustness in a multilayer heterogeneous biological network (11). Moreover, merely counting the number of feedback loops in the network is insufficient to capture the overall network topology, as these feedback loops can be coupled to varying degrees. Consequently, more sophisticated measures need to be developed that take into account the location and degree of interaction between different feedback loops to more effectively understand which loops must be disrupted for maximum effect. Other topological factors, such as high interconnectivity, redundancy, and degree distribution, can also influence robustness (51,52). Despite these limitations, our results provide an integrated platform to understand the structural and dynamic robustness of EMP. Understanding the interplay between NPLs and PFLs that lend these networks robustness, as well the mutations that can expose the fragility of these networks is crucial for drug design from a therapeutic perspective.

METHODS

Random network generation

Random networks were generated uniformly across the set of all connected networks. We generated 100 random networks for each size, defined by the number of nodes in the network $n = 4 - 10$. The total number of edges in the network is decided before generation (m) with the constraint $m \geq n - 1$, and picked uniformly from the binomial distribution:

$$P_m = \left(\binom{n}{2} \right) 0.5^m.$$

First a random spanning tree (a graph on the n nodes without any cycle with $n - 1$ edges) is generated by picking edges uniformly at random, and adding them if they do not cause a cycle, ensuring that each node is connected with another node in the network. The remaining edges ($m - n+ 1$) are then added randomly until the desired total number of edges is reached. The random networks generated for calculating pJSD have an additional condition: each node of the network must have an outgoing edge. This is to ensure that there are no output nodes that unduly change the JSD despite the core network dynamics not changing.

The network sizes we analyze for each criteria of robustness are as follows:

average pJSD: $4 - 8$
average fold change in plasticity (dynamic): $4 - 8$
average parameter variation JSD: $4 - 8$
average fold change in plasticity (structural): $4 - 5$
JSD between RACIPE and CSB: $4 - 8$

Analysis for larger networks could be performed for criteria that only use the CSB, but those that also use RACIPE faced computational limitations, especially structural robustness in plasticity, as multiple perturbed networks need to be simulated for each network topology. The above data sets were generated in triplicates, and analysis performed in parallel. The corresponding measures are available in Table 2.

CSB formalism

CSB formalism is based on the Boolean model by Font-Clos et al. (33), but with a continuous state space. In this model, the expression values of the

TABLE 2 WT Percentiles in the corresponding random network distributions for different measures of robustness

Robustness measures	Run1	Run2	Run3	Average	SD
GRHL2					
DJSD	0.096	0.202	0.212	0.17	0.06
DPLAST	0.885	0.808	0.827	0.84	0.04
PPLAST	0.558	0.625	0.635	0.61	0.04
PJSD	0.125	0.202	0.183	0.17	0.04
DJSD2	0.077	0.087	0.067	0.08	0.01
GRHL2wa					
DJSD	0.058	0.154	0.154	0.12	0.06
DPLAST	0.779	0.721	0.721	0.74	0.03
PPLAST	0.875	0.923	0.933	0.91	0.03
PJSD	0.048	0.106	0.067	0.07	0.03
DJSD2	0.26	0.317	0.269	0.28	0.03
OVOL					
DJSD	0.067	0.202	0.202	0.16	0.08
DPLAST	0.971	0.904	0.923	0.93	0.03
PPLAST	0.654	0.702	0.692	0.68	0.03
PJSD	0.288	0.385	0.365	0.35	0.05
DJSD2	0.135	0.125	0.135	0.13	0.01
OVOLsi					
DJSD	0.125	0.212	0.24	0.19	0.06
DPLAST	0.923	0.856	0.885	0.89	0.03
PPLAST	0.702	0.76	0.721	0.73	0.03
PJSD	0.173	0.25	0.202	0.21	0.04
DJSD2	0.048	0.067	0.019	0.04	0.02
OCT4					
DJSD	0.198	0.188	0.208	0.20	0.01
DPLAST	0.941	0.812	0.891	0.88	0.07
PPLAST	0.703	0.822	0.802	0.78	0.06
PJSD	0.01	0.02	0	0.01	0.01
DJSD2	0.01	0.01	0.01	0.01	0.00
NRF2					
DJSD	0.267	0.386	0.406	0.35	0.08
DPLAST	0.891	0.713	0.861	0.82	0.10
PJSD	0.248	0.248	0.198	0.23	0.03
DJSD2	0.02	0.02	0.01	0.02	0.01

nodes in a GRN are continuous real values restricted between $[-1, 1]$ (1 corresponding to ON and -1 corresponding to OFF). The update rule is formulated to be similar to the Euler integration method. The rate of change in the expression level is modeled as a sigmoidal function, as follows:

$$x_i^{t+1} = x_i^t + \Delta t \frac{A_i^t}{|A_i^t| + 1},$$

where x_i^t is the expression of node i at time t, A_i^t is the activation of node i at time t, defined as:

$$A_i^t = \sum_{j \in N_i} x_j^t J_{ji},$$

where N_i is the set of nodes activating/inhibiting node i, J_{ji} is the sign of the edge from node j to node i. $\Delta t = 0.1$ corresponds to a small discrete time step. Upper and lower bounds of -1 and 1 are enforced on the expression levels during the simulations, such that, if x_i^{t+1} goes below -1 (or goes above 1), x_i^{t+1} is set to -1 (or 1). A state at time t is classified as stable or unstable based on the following condition:

$$\text{if } \left(A_i^t x_i^t < 0\right) \text{ AND } \left(|A_i^t| \geq 0.25 D_i^{0.5}\right) \text{ for any node } i \text{ then the state is not stable,}$$

where D_i is the indegree of node i. The condition can be described as follows: if the activation of any node has an opposite sign as the expression level of the node (thereby pushing the node toward the opposite sign), and if the activation is large enough for the push to be of any consequence, then the state is unstable. The lower bound for the activation threshold ($0.25 D_i^{0.5}$) is of the order of the standard deviation of activation of a node, if input nodes were randomly initialized. Essentially, we only consider the state to be unstable if the sign of some node does not match its activation, AND the activation is sufficiently large in modulus. The networks are simulated until a stable state is reached. The stable state values are then binarized as 1 for positive stable state and 0 otherwise.

Calculating steady-state frequency distributions

As mentioned earlier, steady-state frequency distributions for RACIPE are calculated over all parameter sets, weighted by the fraction of initial conditions that converge to that state for each parameter set. For Boolean and CSB formalisms, we calculate the frequency of each steady state across all simulations with random initial conditions. These steady-state frequency distributions are then used to calculate the JSD that measures robustness in distribution.

JSD

The difference between two phenotypic distributions can be quantified by the JSD metric. For two discrete frequency distributions $P(x)$ and $Q(x)$, we define:

$$\text{JSD}(P||Q) = \frac{1}{2} D(P||M) + \frac{1}{2} D(Q||M),$$

where $M = \frac{P+Q}{2}$, and D is the Kullback-Leibler divergence, given by:

$$D(P||Q) = \sum_x P(x) log \frac{P(x)}{Q(x)}.$$

JSD varies from 0 to 1 when base two is used to calculate the logarithm in D, with 0 indicating that the distributions are identical, and 1 indicating that the distributions have no overlap. The JSD values were calculated using the jensenshannon function in the scipy.spatial.distance module (Python 3.8).

Fold change in plasticity

Fold change in plasticity is used to measure the degree of change in plasticity of the WT upon a perturbation, either dynamic or structural. If the plasticity of the WT network is p_1 and the plasticity of the perturbed network is p_2, then:

$$\text{Fold Change} = min\left(\frac{p_1}{p_2}, \frac{p_2}{p_1}\right).$$

Consequently, the fold change ranges from 0 to 1, and a higher value indicates that the perturbed network has plasticity closer to the WT. Hence, looking at the average fold change due to perturbation (structural, or kinetic parameter variation) gives a good estimate of the robustness in plasticity of the network.

Comparison of parameter variation curves for plasticity

To understand how important of a role the hill coefficient plays in the kinetic variation of a network, we expanded/shrunk the parameter space in three different regimes: all parameters varied simultaneously, with everything but the Hill coefficient being varied. The absolute area between the control (all parameters) and the second and third regimes were then computed to quantify the closeness of the parameter variation schemes, with a lower value indicating that the curves are more similar.

Calculating the number of feedback loops

The number of feedback loops in a given network was calculated using the NetworkX package (53). We first count the number of cycles in the network using the *simple_cycles* function, then traverse through each cycle multiplying the edge signs up (1 for activation and -1 for inhibition). The cycle is classified as a PFL if the product is positive and negative otherwise.

Weighting of feedback loops

We weigh the PFLs and NFLs, thereby defining WPFLs and WNFLs as follows:

$$\text{WPFL} = \sum_i \frac{1}{\text{length } (i)}$$

$$\text{WNFL} = \sum_j \frac{1}{\text{length } (j)}.$$

Fraction of positive cycles (unweighted and weighted)

The FPC in the network is simply given by

$$FPC = \frac{PFL}{PFL + NFL}$$

Similar to the above, one can also weight the cycles (by length and sign) when calculating the FWPC:

$$FWPC = \frac{w \cdot WPFL}{w \cdot WPFL + WNFL},$$

where w is the weight assigned to WPFLs to improve the correlation with robustness measures. $w = 1$ by default.

Statistical tests and functions

All correlation analysis was done using the Spearman correlation method using the scipy.stats.pearsonr module. The corresponding statistical significance values are represented by '*', to be translated as: *p $<$ 0.05, **p $<$ 0.01, ***p $<$ 0.001. Unpaired t test for the violin plots was performed using the scipy.stats.ttest_ind function, with significance being reported as above. Regression bands (95% CI) for correlation plots were plotted using seaborn.regplot.

DATA AND CODE AVAILABILITY

The raw data generated for this study are available at https://bit.ly/3iHZBSd. Derived data sets and code supporting the current findings, including the codes for the continuous Boolean model, and codes to generate SBML models of the networks, are available on the github page: https://github.com/csbBSSE/Robustness_project.

Additional information

Correspondence and requests for materials should be addressed to M.K.J.

SUPPORTING MATERIAL

Supporting material can be found online at https://doi.org/10.1016/j.bpj.2022.07.017.

AUTHOR CONTRIBUTIONS

M.K.J. conceived and supervised the research. A.H., A.M., and K.H. performed the research and analyzed the results. All authors prepared the manuscript.

ACKNOWLEDGMENTS

A.H. and A.M. are supported by the KVPY fellowship awarded by the Department of Science and Technology (DST), Government of India. K.H. is supported by the Prime Ministers Research Fellowship (PMRF). M.K.J. is supported by the Ramanujan Fellowship (SB/S2/RJN 049/2018) awarded by the Science and Engineering Research Board (SERB), DST, Government of India. Mr. Atchuta Srinivas Duddu is acknowledged for artwork (Figs. 1, *a*, *e* and 3 *a*).

DECLARATION OF INTERESTS

The authors declare no competing interests.

REFERENCES

1. Kirschner, M., and J. Gerhart. 1998. Evolvability. *Proc. Natl. Acad. Sci. USA.* 95:8420–8427.
2. Kitano, H. 2004. Biological robustness. *Nat. Rev. Genet.* 5:826–837.
3. de Visser, J. A., J. Hermisson, G. P. Wagner…, 2003. Evolution and detection of genetic robustness. *evolution.* 57:1959.
4. Holling, C. S. 2001. Understanding the complexity of economic. *Ecosystems.* 4:390–405.
5. Kitano, H. 2007. Towards a theory of biological robustness. *Mol. Syst. Biol.* 3:137.
6. Whitacre, J. M. 2012. Biological robustness: paradigms, mechanisms, systems principles. *Front. Genet.* 3:67.
7. Waddington, C. H. 1942. Canalization of development and the inheritance of acquired characters//Nature. *Nature.* 150:563–565.
8. Baggio, J. A., S. B. BurnSilver, M. De Domenico…, 2016. Multiplex social ecological network analysis reveals how social changes affect community robustness more than resource depletion. *Proc. Natl. Acad. Sci. USA.* 113:13708–13713.
9. Potts, M. W., P. A. Sartor, …, S. Bullock. 2020. A network perspective on assessing system architectures: robustness to cascading failure. *Syst. Eng.* 23:sys.21551–sys.21616.
10. Larhlimi, A., S. Blachon, Z. Nikoloski…, 2011. Robustness of metabolic networks: a review of existing definitions. *Biosystems.* 106:1–8.
11. Liu, X., E. Maiorino, …, A. Sharma. 2020. Robustness and lethality in multilayer biological molecular networks. *Nat. Commun.* 11:6043.
12. Macneil, L. T., and A. J. M. Walhout. 2011. Gene regulatory networks and the role of robustness and stochasticity in the control of gene expression//Genome Research. *Genome Res.* 21:645–657.
13. Rodrigues, F. A., L. d. F. Costa, and A. L. Barbieri. 2011. Resilience of protein-protein interaction networks as determined by their large-scale topological features. *Mol. Biosyst.* 7:1263–1269.
14. Gates, A. J., R. B. Corriea, L. M. Rocha…, 2021. The effective graph reveals redundancy, canalization, and control pathways in biochemical regulation and signaling. *Proc. Natl. Acad. Sci. USA.* 118:148–162.
15. Barabási, A. L., and Z. Oltvai. 2004. Network biology: understanding the cell's functional organization. *Nat. Rev. Genet.* 5:101–113.
16. Kauffman, S. 1974. The large scale structure and dynamics of gene control circuits. *J. Theor. Biol.* 44:167–190.
17. Bashan, A., Y. Berezin, …, S. Havlin. 2013. The extreme vulnerability of interdependent spatially embedded networks. *Nat. Phys.* 9:667–672.
18. Liu, X., H. E. Stanley, and J. Gao. 2016. Breakdown of interdependent directed networks. *Proc. Natl. Acad. Sci. USA.* 113:1138–1143.
19. Kwakernaak, H. 1983. Robustness Optimization of linear feedback systems. *Decis. Control.* 2:618–624.
20. Pritchard, A. J., and S. Townley. 1989. Robustness of linear systems. *J. Differ. Equ.* 77:254–286.
21. Carlson, J. M., and J. Doyle. 2000. Highly optimized tolerance: robustness and design in complex systems. *Phys. Rev. Lett.* 84:2529–2532.
22. Jeong, H., S. P. Mason, …, Z. N. Oltvai. 2001. Lethality and centrality in protein networks. *Nature.* 411:41–42.
23. Navlakha, S., X. He, …, Z. Bar-Joseph. 2014. Topological properties of robust biological and computational networks. *J. R. Soc. Interface.* 11:20140283.
24. Kalluri, R., and R. A. Weinberg. 2009. The basics of epithelial-mesenchymal transition. *Journal of Clinical Investigation.* 119:1420–1428.
25. Tsai, J. H., and J. Yang. 2013. Epithelial–mesenchymal plasticity in carcinoma metastasis. *Genes & Development.* 27:2192–2206.
26. Hari, K., B. Sabuwala, M. K. Jolly…, 2020. Identifying inhibitors of epithelial–mesenchymal plasticity using a network topology-based approach. *npj Systems Biology and Applications.* 6:1–15.
27. Watanabe, K., N. Panchy, T. Hong…, 2019. Combinatorial perturbation analysis reveals divergent regulations of mesenchymal genes during epithelial-to-mesenchymal transition. *npj Syst. Biol. Appl.* 5:21.
28. Zhang, J., X.-J. Tian, J. Xing…, 2014. TGF-β–induced epithelial-to-mesenchymal transition proceeds through stepwise activation of multiple feedback loops. *Sci. Signal.* 7:ra91.
29. Jain, P., S. Bhatia, M. K. Jolly…, 2022. Population dynamics of epithelial-mesenchymal heterogeneity in cancer cells. *Biomolecules.* 12:348.

30. Pastushenko, I., A. Brisebarre, C. Blanpain…, 2018. Identification of the tumour transition states occurring during EMT. *Nature.* 556:463–468.

31. Lin, J. 1991. Divergence measures based on the Shannon entropy. *IEEE Trans. Inf. Theory.* 37:145–151.

32. Huang, B., M. Lu, …, J. N. Onuchic. 2017. Interrogating the topological robustness of gene regulatory circuits by randomization. *PLoS Comput. Biol.* 13:e1005456.

33. Font-Clos, F., S. Zapperi, and C. A. M. La Porta. 2018. Topography of epithelial–mesenchymal plasticity. *Proc. Natl. Acad. Sci. USA.* 115:5902–5907.

34. Kwon, Y. K., and K. H. Cho. 2007. Boolean dynamics of biological networks with multiple coupled feedback loops. *Biophys. J.* 92:2975–2981.

35. Kwon, Y. K., and K. H. Cho. 2008. Quantitative analysis of robustness and fragility in biological networks based on feedback dynamics//Bioinformatics. *Bioinformatics.* 24:987–994.

36. Pinho, R., V. Garcia, M. W. Feldman…, 2014. Stability Depends on positive Autoregulation in boolean gene regulatory networks. *PLoS Comput. Biol.* 10:e1003916.

37. Feliu, E., and C. Wiuf. 2015. Finding the positive feedback loops underlying multi-stationarity. *BMC Syst. Biol.* 9:22.

38. Seo, C. H., J. R. Kim, K.-H. Cho…, 2009. Hub genes with positive feedbacks function as master switches in developmental gene regulatory networks. *Bioinformatics.* 25:1898–1904.

39. Huang, B., D. Jia, …, M. Lu. 2018. RACIPE: A computational tool for modeling gene regulatory circuits using randomization. *BMC Syst. Biol.* 12:1–74.

40. Jia, D., J. T. George, …, H. Levine. 2019. Testing the gene expression classification of the EMT spectrum. *Phys. Biol.* 16:025002.

41. Jolly, M. K., T. C. Tripathi, H. Levine…, 2016. Stability of the hybrid epithelial/mesenchymal phenotype. *Oncotarget.* 7:27067–27084.

42. Celià-Terrassa, T., C. Bastian, Y. Kang…, 2018. Hysteresis control of epithelial-mesenchymal transition dynamics conveys a distinct program with enhanced metastatic ability. *Nat. Commun.* 9:5005.

43. Rashid, M., K. Hari, M. K. Jolly…, 2022. Network topology metrics explaining Enrichment of hybrid epithelial mesenchymal phenotypes in metastasis. Preprint at bioRxiv. https://doi.org/10.1101/2022.05.16.492000.

44. Ingolia, N. T. 2004. Topology and robustness in the Drosophila segment polarity network. *PLoS Biol.* 2:e123.

45. von Dassow, G., M. Eli, G. M. Odell…, 2000. The segment polarity network is a robust developmental module. *Nature.* 406:188–192.

46. Isalan, M., C. Lemerle, L. Serrano…, 2008. Evolvability and hierarchy in rewired bacterial gene networks. *Nature.* 452:840–845.

47. Nagata, S., and M. Kikuchi. 2020. Emergence of cooperative bistability and robustness of gene regulatory networks. *PLoS Comput. Biol.* 16:e1007969.

48. Burda, Z., A. Krzywicki, M. Zagorski…, 2011. Motifs emerge from function in model gene regulatory networks. *Proc. Natl. Acad. Sci. USA.* 108:17263–17268.

49. Kwon, Y. K., and K. H. Cho. 2008. Coherent coupling of feedback loops: a design principle of cell signaling networks. *Bioinformatics.* 24:1926–1932.

50. Hari, K., V. Ullanat, M. K. Jolly…, 2021. Landscape of Epithelial Mesenchymal Plasticity as an emergent property of coordinated teams in regulatory networks. Preprint at bioRxiv. https://doi.org/10.1101/2021.12.12.472090.

51. Albert, R., H. Jeong, and A. L. Barabási. 2000. Error and attack tolerance of complex networks. *Nature.* 406:378–382.

52. Ichinose, N., T. Yada, and H. Wada. 2018. Asymmetry in indegree and outdegree distributions of gene regulatory networks arising from dynamical robustness. *Phys. Rev. E.* 97:062315.

53. Hagberg, A., S. Pieter, and S. C. Daniel. 2008. Exploring Network Structure, Dynamics, and Function Using NetworkX. Proceedings of the 7th Python in Science Conference, pp. 11–15. Pasadena, CA, USA.